Modeling Ventricular Excitation : axial and orthotropic anisotropy effects on wavefronts and potentials.

Piero Colli–Franzone, Luciano Guerri[*] *and Bruno Taccardi*[+]

Dipartimento di Matematica, Università di Pavia
Istituto di Analisi Numerica del C.N.R, Pavia
[*] Università del Piemonte Orientale, Alessandria
[+] C.V.R.T.I. University of Utah, Salt Lake City, UT

1 Abstract

By applying the eikonal approximation to the bidomain model of the cardiac tissue we investigate the influence of the axially isotropic and orthotropic conductivity tensors on the propagation of the excitation wave fronts and on the associated potential distribution and electrograms.

2 Introduction

In recent years the effects of the anisotropic structure of the myocardial tissue on the spread of excitation in the heart were investigated in depth, see e.g. [10, 6, 3, 12]. These studies showed that the anisotropic spread of excitation, the potential distributions and the shape of the EGs (electrograms) are strongly influenced by the direction and intramural rotation of the myocardial fibers, by the anisotropy ratios of the intra and extra cellular conductivities, by the presence of extracardiac conducting media and by the reference potential. The modeling and simulation of the excitation process are important tools for studing the anisotropic motion of the excitation wave front and for testing the validity of many proposed criteria for the interpretation of experimental data, [10] e.g., the shapes of the epicardial and intramural QRS complexes and the configurations of the epicardial and intramural potential distributions.

In [2, 12] the influence of the rotational anisotropy in a large slab modeling the myocardial wall was investigated and in [3, 6] the simulations were extended to an anisotropic model of the left ventricle with ellipsoidal geometry. In agreement with experimental findings, these studies showed that excitation spreads faster along than across fibers and the QRS waveforms vary from monophasic to polyphasic as a function of position of the unipolar electrode; more precisely, epicardial pacing gives rise to R waves or to Q waves, humps and spikes, in EGs recorded from points reached by excitation wave fronts that move along or across fibers.

In most previous simulations it was assumed that the conductivity tensors are *axially isotropic*, i.e. each media *(i), (e)* has the same conductivity cofficients along any cross-fiber directions.

Recently in [8] it was shown that the architecture of the ventricular muscle fibers and of the extracellular connective tissue matrix suggests a laminar organization of the ventricular myocardium which would entails *orthotropic* conductivity tensors. These studies challenge the assumption of *axially isotropic* conductivity tensors. An orthotropic simulation, related to endocardial pacing, is described in[17].

In the present paper we use our previously described model of the left ventricle[3] to investigate the influence of *orthotropic conductivity tensors* on the epicardial excitation sequence and on the associated potentials, elicited by epicardial stimulus.

3 The eikonal approach

We briefly sketch the *eikonal approach* developed in [3] and we describe its extension to the *orthotropic tensors framework*; the *eikonal approach* was used in [3, 6], assuming *axially isotropic tensors*, for large scale simulations of the excitation sequences, the potential patterns and electrograms and is based on a macroscopic analysis of the so called *bidomain model* [11]. In the macroscopic bidomain representation of the cardiac tissue, the anisotropic structure of the two averaged continuous media, the intra and the extracellular medium, are characterized by the conductivity tensors M_i and M_e. The anisotropic conductivity is related to the arrangement of the cardiac fibers, whose direction rotates counterclockwise from the epicardium to the endocardium see [16].

From [8] it follows that the ventricular myocardium may be conceived as a set of muscle sheets running radially from epi to endocardium. In this laminar organization it is possible to identify three distinct principal axes at any point $\mathbf{x}$. Let $\mathbf{a}_l,\ \mathbf{a}_t,\ \mathbf{a}_s$ be a triplet of orthonormal vectors related to the structure of the myocardium, with $\mathbf{a}_l$ parallel to the local fiber direction. This triplet may depend on the position $\mathbf{x}$ in the myocardium. Let $\sigma_l^{i,e},\ \sigma_t^{i,e},\ \sigma_s^{i,e}$ be the conductivity coefficients mesured along the corresponding directions. Then the conductivity tensors M_i and M_e, generally dependent on the position $\mathbf{x}$, are given by:

$$M_{i,e}(\mathbf{x}) = \sigma_l^{i,e}\ \mathbf{a}_l(\mathbf{x})\mathbf{a}_l^T(\mathbf{x}) + \sigma_t^{i,e}\ \mathbf{a}_t(\mathbf{x})\mathbf{a}_t^T(\mathbf{x}) + \sigma_s^{i,e}\ \mathbf{a}_s(\mathbf{x})\mathbf{a}_s^T(\mathbf{x}) \tag{1}$$

if $\sigma_s^{i,e} = \sigma_t^{i,e}$ we recover the axially isotropic case. Imposing the conservation of currents, i.e. the interchange between the two media must balance the membrane current flow per unit volume, one derives a reaction-diffusion system defined in the cardiac tissue; denoting $\mathbf{J}_i = -M_i\nabla u_i$, $\mathbf{J}_e = -M_e\nabla u_e$ the intra and extracellular current densities, in terms of the intra and extracellular potentials $u_i(\mathbf{x},t),\ u_e(\mathbf{x},t)$, we have the following reaction-diffusion system in the myocardial tissue H :

$$\begin{cases} c_m\ \partial_t(u_i - u_e) - \text{div}\ M_i\nabla u_i + \ i_{ion} = 0 \quad \text{in } H \\ c_m\ \partial_t(u_e - u_i) - \text{div}\ M_e\nabla u_e - \ i_{ion} = 0 \quad \text{in } H \end{cases} \tag{2}$$

with c_m and i_{ion} the capacitance and ionic current membrane per unit volume. When a suitable stimulus is applied the presence of a slow *diffusion* and fast *reaction* terms forces the development of a propagating excitation interface associated to a fast transition of the transmembrane potential $v(\mathbf{x},t) = u_i(\mathbf{x},t) - u_e(\mathbf{x},t)$ from the resting v_r to the excited or plateau v_p value. Since the excitation phase v exhibits a monotonic time behavior we introduce the *activation time* $\varphi(\mathbf{x})$ as the time instant at which $v(\mathbf{x},\varphi(\mathbf{x}))$=($v_r$ + v_p)/2; then we define the excitation wavefront as the level surface of the activation time:

$$S(t) = \ \{\mathbf{x} \in H,\ \ \varphi(\mathbf{x}) = t\} \tag{3}$$

In order to describe the *wavefront motion* we introduce the intra and extra conductivity coefficients measured along the direction $\boldsymbol{\xi}$ given by : $\sigma_{i,e}(\mathbf{x},\boldsymbol{\xi}) = \boldsymbol{\xi}^T M_{i,e}(\mathbf{x})\boldsymbol{\xi}$ with $\boldsymbol{\xi}^T\boldsymbol{\xi} = 1$; then we denote by $\sigma(\mathbf{x},\boldsymbol{\xi}) = (\sigma_i(\mathbf{x},\boldsymbol{\xi})^{-1} + \sigma_e(\mathbf{x},\boldsymbol{\xi})^{-1})^{-1}$ the harmonic mean of $\sigma_{i,e}(\mathbf{x},\boldsymbol{\xi})$. Finally we define the following *Anisotropic Indicatrix*:

$$\Phi(\mathbf{x},\boldsymbol{\xi}) = \sqrt{\sigma(\mathbf{x},\boldsymbol{\xi})} \tag{4}$$

For a cardiac tissue fully recovered and instantaneous ionic membrane current i_{ion}, i.e. $i_{ion} = F(v)$, in [2] we investigated *the asymptotic behavior* of traveling wavefronts solutions of the R–D system; we showed that the velocity of the wavefront $S(t)$ along the Euclidean normal direction $\boldsymbol{\nu}$ is given by $\theta(\mathbf{x}, \boldsymbol{\nu}) = 1/|\nabla\varphi|$ where the activation time $\varphi(\boldsymbol{\xi})$ is a solution of the following *eikonal-diffusion equation*:

$$-\frac{1}{c_m}\,\text{div}\,[\Phi(\mathbf{x}, \nabla\varphi)\Phi_\xi(\mathbf{x}, \nabla\varphi)] + \rho\Phi(\mathbf{x}, \nabla\varphi) = 1 \tag{5}$$

Since the previous *eikonal model* is derived assuming that $M_{i,e}$ are symmetric and positive definite matrices, then (5) is valid also for the *orthotropic case*. The parameter $\rho = 1/\sqrt{\mu}$ is related to the asymptotic velocity of the action potential traveling in an infinite cable, i.e. $(\mu\,,\ A(\tau))$ is the unique bounded solution of the eigenvalue problem:

$$\begin{cases} -\mu\, A'' + c_m\, A' + i_{ion}(\, A) = 0 \\ A(\mp\infty) = v_r \text{ or } v_p, \quad A(0) = (v_p + v_r)/2 \end{cases} \tag{6}$$

and the transmembrane potential $v(\mathbf{x}, t)$ is approximated by $v(\mathbf{x}, t) = A(t - \varphi(\mathbf{x}))$ Since the propagating front during the excitation phase admits a Cartesian representation, the previous eikonal–diffusion equation proved to be more convenient for computational purposes than other eikonal approximations [1, 9]. We remark that the *activation time* $\tau = \varphi(\mathbf{x})$ is a smooth function, therefore the numerical simulation of the *eikonal equation* can be performed on a quasi-uniform grid with mesh size greater than 1-2 mm. This allows a strong reduction of the computational complexity with respect to the R-D system, when performing large scale simulations with a view to obtaining a qualitative macroscopic description of the excitation phase in a normal ventricle.
The knowledge of $v(\mathbf{x}, t) = A(t - \varphi(\mathbf{x}))$ allows to simulate the time – space extracellular potential on the QRS complex.
In the following we shall denote by H the heart tissue, by Ω_b and σ_b the cavitary blood and its conductivity, by Ω_f and σ_f the fluid volume adjacent to the epicardium and its conductivity, by $\Omega_0 = \Omega_b \cup \Omega_f$ the whole extracardiac medium in contact with H and by $\bar{\Omega} = \bar{H} \cup \bar{\Omega}_0$. Let $\Gamma = \partial\Omega\,, \Gamma_H = \Gamma \cap \partial H, \Gamma_0 = \Gamma \cap \partial\Omega_0$ and $\Sigma = \partial H \cap \partial\Omega_0$, i.e. Σ represents the parts of the epi and/or endocardium in contact with Ω_0. In particular the epicardial surface will be denoted by Σ_{epi}. Denoting by M_0 and by u_0 the conductivity tensor and potential in the extra-cardiac domain we set:

$$\widehat{M} = \begin{cases} M_i(\mathbf{x}) + M_e(\mathbf{x}) \\ M_0(\mathbf{x}) \end{cases} \quad u(\mathbf{x}, t) = \begin{cases} u_e(\mathbf{x}, t) & \mathbf{x} \in H \\ u_0(\mathbf{x}, t) & \mathbf{x} \in \Omega_0 \end{cases} \quad \mathbf{J}_v(\mathbf{x}, t) = -M_i \nabla v(\mathbf{x}, t)$$

Denoting by $\mathbf{J}_i,\ \mathbf{J}_e,\ \mathbf{J}_0$ the intra, extracellular and extracardiac current densities respectively and assuming that the extracardiac medium is insulated, then applying the current conservation we have :

$$\begin{cases} \text{div}\,(\mathbf{J}_i + \mathbf{J}_e) = 0 \ \text{ in } H \\ \mathbf{n}^T(\mathbf{J}_i + \mathbf{J}_e) = \mathbf{n}^T\mathbf{J}_0 \ \text{ on } \Sigma \text{ and } \Gamma_H, \end{cases} \qquad \begin{cases} \text{div}\,\mathbf{J}_0 = 0 \ \text{ in } \Omega_0 \\ \mathbf{n}^T\mathbf{J}_0 = 0 \ \text{ on } \Gamma_0 \end{cases} \tag{7}$$

recalling that $\mathbf{J}_i = -M_i\nabla u_i,\ \mathbf{J}_e = -M_e\nabla u_e$ and $\mathbf{J}_0 = -M_0\nabla u_0$ then in terms of the extracellular or extracardiac potential $u(\mathbf{x}, t)$ the equations (7) are equivalent to the following differential formulation of the *Bidomain Potential Model*:

$$\begin{cases} \text{div}\,\widehat{M}\nabla u(\mathbf{x}, t) = \begin{cases} \text{div}\,\mathbf{J}_v(\mathbf{x}, t) & \text{in } H \\ 0 & \text{in } \Omega_0 \end{cases} \\ [\![\ u(\mathbf{x}, t)\ ]\!]_\Sigma = 0 \qquad [\![\ \mathbf{n}^T\widehat{M}\nabla u(\mathbf{x}, t)\ ]\!]_\Sigma = \mathbf{n}^T\mathbf{J}_v(\mathbf{x}, t) \\ \mathbf{n}^T M_0 \nabla u(\mathbf{x}, t) = 0 \quad \text{on } \Gamma_0 \\ (M\nabla u(\mathbf{x}, t)) \cdot \mathbf{n} = \mathbf{n}^T\mathbf{J}_v(\mathbf{x}, t) \quad \text{on } \Gamma_H \end{cases} \tag{8}$$

where $[\![\ \varphi\ ]\!]_\Sigma$ denotes the jump of φ through Σ, i.e. $[\![\ \varphi\ ]\!]_\Sigma = \varphi_{\Sigma^+} - \varphi_{|\Sigma^-}$ with $\varphi_{|\Sigma^\pm}$ the traces taken on the positive and negative side of Σ with respect to the oriented normal. Therefore problem (8) provides the extracellular or extracardiac potential $u(\mathbf{x}, t)$ from the knowledge of $v(\mathbf{x}, t)$.
Different mathematical approaches can be used to simulate EGs (see e.g. [7, 13]). An integral formulation turns out to be more efficient for simulating accurately a limited number of EGs than differential or variational representations for large scale simulations [5, 13].

Each EG represents the time course of the potential difference between one point of the domain, called observation point, and a *reference potential*. For unipolar EGs, the reference potential is the potential at a remote site or, more frequently, is obtained by averaging the potential values over a set of three or more points or over a surface. Recent experimental observations showed that the potential of Wilson's central terminal is close to the average potential measured on the epicardial ventricular surface [14]. Setting

$$w(\mathbf{x}, t) = u(\mathbf{x}, t) - \frac{1}{|\Sigma_{epi}|} \int_{\Sigma_{epi}} u(\boldsymbol{\xi}, t)\ d\sigma_\xi. \tag{9}$$

we show that the following *integral representation* allows to compute EGs having as reference potential the average potential on the epicardial surface Σ_{epi} the system :

$$w(\mathbf{x}, t) = \int_H {\mathbf{J}_v}^T\ \nabla_\xi \psi(\boldsymbol{\xi}, \mathbf{x})\ d\xi = -\int_H (\nabla v(\boldsymbol{\xi}, t))^T\ M_i(\boldsymbol{\xi}) \nabla_\xi \psi(\boldsymbol{\xi}, \mathbf{x})\ d\xi \tag{10}$$

where the Green function or the so-called *Lead Field* ψ satisfies:

$$\begin{cases} -\mathrm{div}_\xi \widehat{M} \nabla_\xi \psi = \begin{cases} \delta(\boldsymbol{\xi} - \mathbf{x}) & for\ \ \mathbf{x} \in \Omega_0 \cup H \\ 0 & for\ \ \mathbf{x} \in \Sigma \end{cases} \\ [\![\ \mathbf{n}^T \widehat{M} \nabla_\xi \psi\ ]\!]_\Sigma = |\Sigma_{epi}|^{-1} \chi_{\Sigma_{epi}}(\boldsymbol{\xi}) + \begin{cases} 0 & for\ \ \mathbf{x} \in \Omega_0 \cup H \\ \delta(\boldsymbol{\xi} - \mathbf{x}) & for\ \ \mathbf{x} \in \Sigma \end{cases} \\ [\![\ \psi\ ]\!]_\Sigma = 0\ ,\ \ \mathbf{n}^T \widehat{M} \nabla_\xi \psi = 0 \quad \text{on } \Gamma \end{cases} \tag{11}$$

with $\chi_{\Sigma_{epi}}(\boldsymbol{\xi})$ characteristic function of Σ_{epi}. The boundary condition imposed for the "lead field" ψ actually reflects the property that $w(\mathbf{x}, t)$, has zero average on the epicardium Σ_{epi}.

By applying the second Green formula to the couple (u, ψ) in Ω_0 and in H with ψ solution of (11) and adding these two relations we obtain:

$$\begin{aligned} \int_{\Omega_0 \cup H} \left[u\ \mathrm{div}\ \widehat{M} \nabla \psi - \psi\ \mathrm{div}\ \widehat{M} \nabla u \right]\ d\xi = \\ \int_\Gamma u\ \mathbf{n}^T \widehat{M} \nabla \psi\ d\sigma_\xi - \int_\Gamma \psi \mathbf{n}^T \widehat{M} \nabla u\ d\sigma_\xi + \\ + \int_\Sigma [\![\ \mathbf{n}^T \widehat{M} \nabla \psi\ ]\!]_\Sigma\ u\ d\sigma_\xi - \int_\Sigma [\![\ \mathbf{n}^T \widehat{M} \nabla u\ ]\!]_\Sigma\ \psi\ d\sigma_\xi \end{aligned} \tag{12}$$

where the unit normal $\mathbf{n}$ is outward to H or to $\bar{\Omega} = \bar{H} \cup \bar{\Omega}_0$ according as we consider the boundary condition on Σ or on Γ. Taking into account that if $\mathbf{x} \notin \Sigma$, for (11) then

$[\![\ \mathbf{n}^T \widehat{M}\nabla\psi\ ]\!]_\Sigma = -\dfrac{1}{|\Sigma_{epi}|}\ \chi_{\Sigma_{epi}}(\boldsymbol{\xi})$ otherwise, if $\mathbf{x} \in \Sigma$, for (11) $[\![\ \mathbf{n}^T \widehat{M}\nabla\psi)\ ]\!]_\Sigma = -\dfrac{1}{|\Sigma_{epi}|}\ \chi_{\Sigma_{epi}}(\boldsymbol{\xi})\ \delta(\boldsymbol{\xi} - \mathbf{x})$, from (12) we have: $u(\mathbf{x},t) + \int_{\Omega_0 \cup H} \psi$ div $\widehat{M}\nabla u\ d\xi - \int_{\Gamma \setminus \Sigma_{epi}} \psi\ \mathbf{n}^T \widehat{M}\nabla u\ d\sigma_\xi - \int_\Sigma [\![\ (\widehat{M}\nabla u) \cdot \mathbf{n}\ ]\!]_\Sigma\ \psi\ d\sigma_\xi - u_{ref} = 0$ where $u_{ref} = \dfrac{1}{|\Sigma_{epi}|} \displaystyle\int_{\Sigma_{epi}} u\ d\sigma_\xi$. Hence taking into account (8) and denoting by $w(\mathbf{x},t)$ the potential difference with respect to the reference potential chosen, i.e. $w(\mathbf{x},t) = u(\mathbf{x},t) - u_{ref}$, it follows:

$$w(\mathbf{x},t) = -\int_H \psi \text{ div } \mathbf{J}_v\ d\xi + \int_{\partial H} \psi\ \mathbf{n}^T \mathbf{J}_v\ d\sigma_\xi$$

and applying the first Green formula we obtain the integral representation:

$$w(\mathbf{x},t) = \int_H \nabla_\xi \psi^T \mathbf{J}_v\ d\xi = -\int_H \nabla_\xi \psi^T M_i \nabla v\ d\xi \tag{13}$$

The boundary condition imposed on the *lead field* actually reflects the property that $w(\mathbf{x},t)$, defined by (9), has zero average on the epicardium. In [5] a rigorous derivation of the integral representation of w is given only when the reference potential is the potential at fixed point $\mathbf{x}_0$ of Ω.

4 Results

By assuming axially isotropic tensors and unequal anisotropy ratio of the media (*i*) and (*e*), both the *bidomain reaction-diffusion system* (7) and the *eikonal model* were shown, see [12, 3], to reproduce the main qualitative features of the excitation sequences elicited by pacing the ventricular wall in exposed dog hearts [10].

We now compare the propagation and shape of excitation fronts obtained under the assumption of either orthotropic or axially isotropic conductivity tensor. The numerical simulations are performed on a monoventricular model previously used in [3, 6]; the model represents a simplified left ventricular wall shaped as an ellipsoidal volume, symmetric with respect to the vertical z–axis, truncated at the base and at the apex. The ventricular model can be conceived as an assembly of packed ellipsoidal surfaces with fiber direction rotating counterclockwise (CCW) from the epicardial (-45^o) to the endocardial (75^o) surface. We also incorporate the epi- endocardial obliqueness of the fibers by introducing the so called *imbrication angle*, see [16]; thus, the fibers do not lie on the packed ellipsoidal surfaces but intersect them at a small angle. In our model the ventricular cavity is not completely filled by blood and the fluid layer in contact with the epicardium has a thickness varying from 2.5 to 5 mm. We include also a simplified network of Purkinje fibers with ventricular junctions (PVJs); for details on the geometry, on the fiber architecture and the PVJs of our model of the left ventricle see [3]. Therefore most of the essential factors affecting the propagation and associated potentials are present in both the experimental setting (exposed hearts in situ or isolated hearts in electrolytic tanks) and in the modeling framework. This allowed us to perform a qualitative comparison between measured and computed potential maps and EGs.

The laminar structure of the ventricular walls observed in [8] is a further anatomical factor that affects cross-fiber conduction on layers parallel to the wall boundary. In this laminar organization it is possible to identify three distinct material axes at any point: one in the direction of the fiber axis which is tangent to a radial muscle sheet, a second perpendicular to the fiber axis and to the sheet and the third one perpendicular to the first two, i.e. tangent to the sheet. The intramural coupling, which occurs through muscle branching across adjacent sheets running approximately in the radial direction, was

estimated to be of relatively low spatial frequency, see [8]. On this basis, it is expected that the intrinsic cross-fiber velocity should be 2 or 3 times greater in the plane of the muscle sheet than perpendicular to it. In our numerical simulations the orthotropic anisotropy is modeled assigning $\mathbf{a}_l$ along the fiber direction and $\mathbf{a}_s$ perpendicular to $\mathbf{a}_l$ and tangent to the ellipsoidal surface through $\mathbf{x}$. The unit vector $\mathbf{a}_t$ is then uniquely determined by the orthogonality condition to $\mathbf{a}_l,\ \mathbf{a}_s$. In [8] the fiber direction $\mathbf{a}_l$ and the surface through $\mathbf{x}$, called radial sheet, connecting the epi- and endocardium, are assigned. $\mathbf{a}_l$ and $\mathbf{a}_s$ are respectively tangent and perpendicular to the radial sheet; the transverse unit vector $\mathbf{a}_t$ is again uniquely determined by the orthogonality condition to $\mathbf{a}_l,\ \mathbf{a}_s$ and is tangent to the radial sheet. The difference between the two implementations of orthotropic conductivity lies then in the choice of the surfaces to which $\mathbf{a}_s$ is tangent or perpendicular. The conductivity coefficients, in $\Omega^{-1}\ cm^{-1}$, used in the orthotropic simulations are :

$$\sigma_l^e = \text{2.e-3} \qquad \sigma_t^e = \text{1.3514e-3} \qquad \sigma_l^i = \text{3.e-3} \qquad \sigma_t^i = \text{3.1525E-4}$$
$$\sigma_s^e = r_e\sigma_t^e, \qquad \sigma_t^i = r_i\sigma_t^i \qquad \text{with} \quad r_e = 0.5 \quad \text{and} \quad r_i = 0.1$$

In the axially isotropic condition $r_{i,e} = 1$, i.e. $\sigma_s^{i,e} = \sigma_t^{i,e}$. In this case we remark that from $\mathbf{a}_l\ \mathbf{a}_l^T + \mathbf{a}_t\ \mathbf{a}_t^T + \mathbf{a}_s\ \mathbf{a}_s^T = I$ it follows that $\mathbf{a}_t\ \mathbf{a}_t^T + \mathbf{a}_s\ \mathbf{a}_s^T = I - \mathbf{a}_l\ \mathbf{a}_l^T$ and $M_{i,e} = \sigma_t^{i,e} I + (\sigma_l^{i,e} - \sigma_t^{i,e})\mathbf{a}_l\ \mathbf{a}_l^T$. Moreover the blood layer has conductivity of $\sigma_b = 6.e-3\ \Omega^{-1} cm^{-1}$ and for the fluid layer, in contact with the epicardial surface, $\sigma_f = 2.e{-}3\ \Omega^{-1}\text{cm}^{-1}$. We remark that for simulating a relatively small number of EGs free from numerical artifacts the *differential representation* is not convenient since it requires a sequence of meshes which dynamically track the propagating excitation layers, which is not an easy task in a 3D environment. In the *integral representation* the *lead field* function ψ is *singular* at the observation point $\mathbf{x}$; therefore to obtain EGs free from numerical artifacts a fixed *adaptive mesh* around the singular point must be used coupled with an *adaptive sub-element technique*, for elements near or inside the excitation layer, in the computation of the integral on H, see [5].

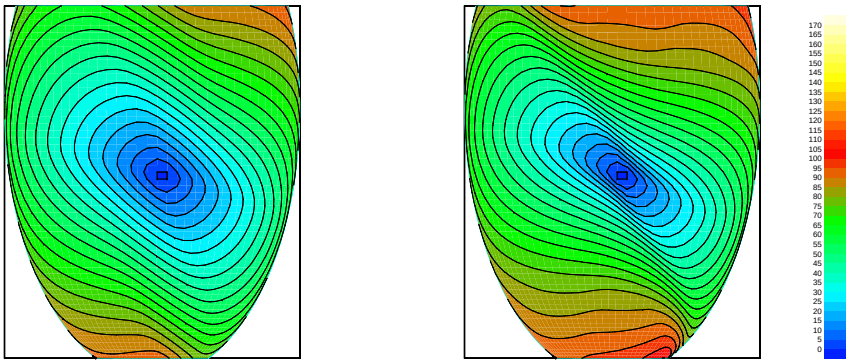

FIGURE 1. Monoventricular model. Central epicardial stimulation: simulated excitation time map depicting the spread of excitation on the epicardial surface for the *axially isotropic* case (left panel) and for the *orthotropic* case (right panel). Time interval between successive isochrones is 5 msec.

Disregarding curvature effects, from (5) it follows that the wave front velocity at point $\mathbf{x}$ in the direction $\mathbf{n}$ is given by $\theta(\mathbf{x}, \mathbf{n}) = \rho\Phi(\mathbf{x}, \nabla\mathbf{n})$. Denoting by $\theta_l,\ \theta_t,\ \theta_s$ the velocities in the direction $\mathbf{a}_l,\ \mathbf{a}_t,\ \mathbf{a}_s$ we have $\theta_s = \theta_t\sqrt{r_i r_e(\lambda_t + 1)/(r_i\lambda_t + r_e)}$, with $\lambda_t = \sigma_t^i/\sigma_t^e$, and the assigned conductivities implies a velocity θ_s of about 1/3 of the expected velocity θ_t in the radial transverse direction . More precisely it follows that the estimated velocity $\theta_l,\ \theta_t,\ \theta_s$ are $0.065,\ 0.030, 0.0103\ cm\ ms^{-1}$ respectively.

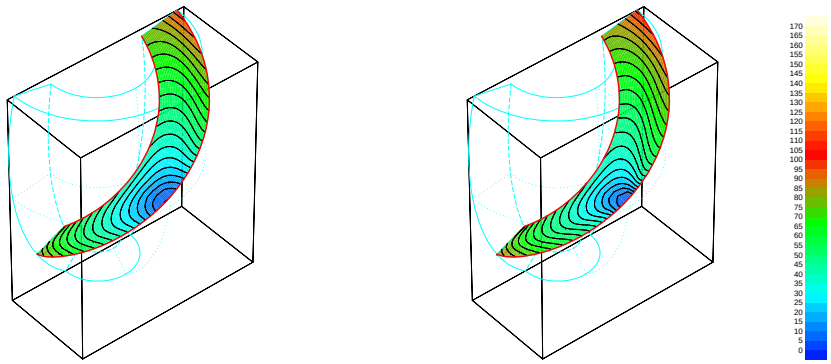

FIGURE 2. Simulated excitation time map on a diagonal intramural surface. Same layout as in Fig. 1.

The results displayed in Figs. 1, 2 allow to compare the sequences of the excitation wave fronts, on the epicardial surface and on an intramural diagonal section passing through the stimulus site, in the axially isotropic and orthotropic cases. We point out only two anisotropic features of the spread of excitation; the epicardial excitation patterns show a family of isochrones lines having oblong and quasi- elliptical shape with the major axes aligned with the epicardial fiber direction. The major difference is that the minor axis of the isochrone, in a cross fiber direction, displayed by the orthotropic case, is less than the minor axis of the axially isotropic case; this is due to the fact that the assigned conductivities implies a velocity θ_s in the direction perpendicular to the fiber and tangent to the elliptic surface of about 1/3 of the expected velocity θ_t in the radial transverse direction. The orthotropic simulation shows that in the cross fiber direction on the epicardial surface the propagation velocities are not as different as one would expect. This unexpected feature is a result of a strong acceleration of the motion of the portions of the wave front mainly propagating across fiber. At about 1 *cm* from the stimulus site in the orthotropic case the velocity is greater than 0.01 $cm\ ms^{-1}$. This effect is due to return of excitation toward the pacing level. Experimental and model data showed that the transmural fiber rotation causes excitation pathways, that start from a pacing site, to first proceed away from it in all directions and then to bend in such a way that they finally point toward the same myocardial level from which they started, whether it be epicardial, midwall or endocardial [4, 15]. One effect of the intramural fiber rotation is that after epicardial pacing, at about 1 *cm* from the pacing site in the cross-fiber direction, the successive intersections of the wave front with the epicardium (epicardial isochrones) indicate a progressively higher velocity of propagation. This is due to the fact that the wavefront intersects the epicardium at an angle smaller than 90 degrees. As a further consequence of fiber rotation, at several *cm* from the pacing site the epicardial isochrones exhibit a dimple-like inflection in the basal and apical part of the wall (Fig. 1).

As shown in Fig. 1, the major difference in the epicardial pattern of excitation lies in the areas separating the regions where the fronts mainly propagates along fiber from those where it propagates across fibers.

We remark that in both cases the posterior isochrones motion is from apex to basis and exhibits a V-shaped pattern converging toward the extinction area; the curvature of the concave V-shaped front causes a faster propagation, see Fig. 4 upper panel, for the orthotropic case and Fig. 8 in [3]-II for the axially isotropic case .

With regard to the simulated epicardial potential distributions, the *Differential Representation* allows us to use a *quasi-uniform grid*, with a rather coarse mesh size, based on the *eikonal model*, in order to obtain fairly accurate results at some distance from the excitation layers (see [3]-II).

In order to take into account the presence of a superficial layer of epicardial, non-muscular tissue of about 200-300 μm of thickness in dog hearts, and also because the extracellular potentials and EGs are measured with electrodes of about of 0.3*mm* in diameter, we compare the anisotropic features displayed by the potential patterns related to the axially-isotropic and orthotropic case simulating the potentials at about 300 μm from the active epicaridal tissue. In both simulations the potential maxima are invariably facing the portion of the wave fronts that move mainly along fibers and create a far-field positivity on the epicardial surfaces.

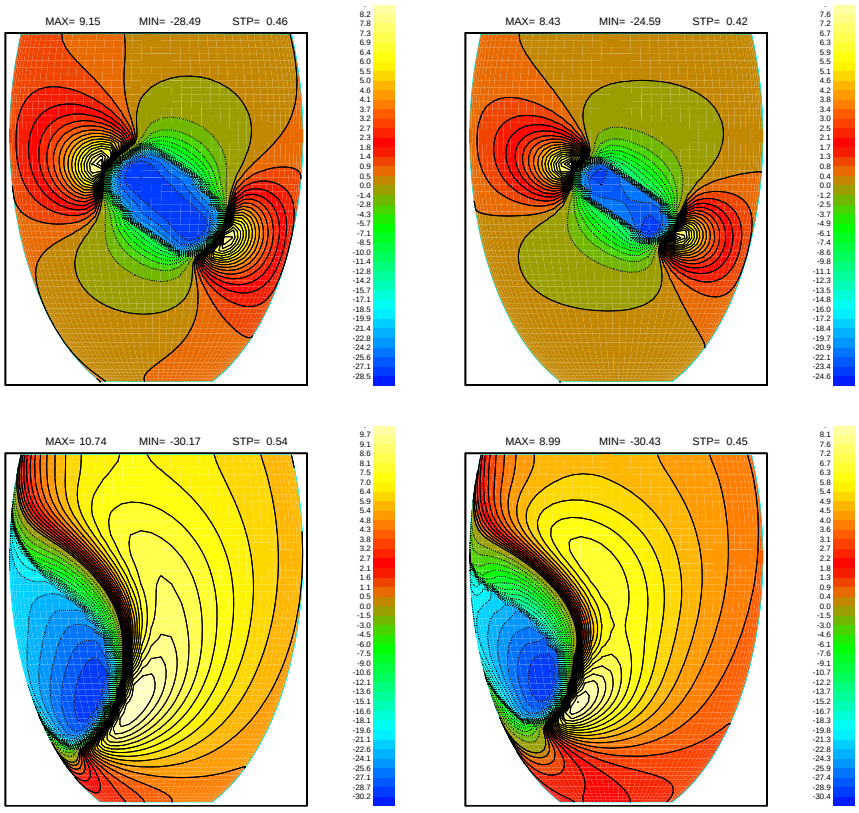

FIGURE 3. Monoventricular model. Central epicardial stimulation: simulated potential maps at about 300 μm from the active myocardial tissue for the *axially isotropic* case (left column) and for the *orthotropic* case (right column). Upper panels: frontal view of the potential map at 20*msec*. Lower panels: lateral view of the potential map at 50 ms; in the lower panels the hearts has been rotated 90^o clockwise for a viewer looking at the heart from above.

At a later stage of the excitation, i.e. at 50 - 60*msec* after the stimulus, the epicardial pattern exhibits again two maxima located ahead of the portion of the wavefront propagating mainly along the epicardial fiber (-45^o); the positive equipotential lines surrounding the maxima undergo a counterclockwise stretching and bending producing

an expanding C-shaped ridge of positivity. This evolution pattern is in part an epicardial reflection of the rotating deep positivity generated by those portions of the wave front which propagate along fibers, whose direction rotates counterclockwise from the epi- to endocardium. The fragmentation of the maxima inside the positive C-shaped strip is more emphasized in the orthotropic simulation.

The anisotropic features such as the location of the potential maxima, the shape of equipotential lines and their evolution are present in both the *axially isotropic* and the *orthotropic* model; therefore from a qualitative point of view, both models are compatible with the experimental findings [10] and only a quantitative comparison with the experimental data could provide a mean for validating one of the two assumptions. Because no substantially different features were observed in the simulations, choosing between the *axially isotropic* or *orthotropic* structure seems a difficul task at present. Another comparison can be performed by analysing the prediction of both models regarding the time course of potentials recorded from specific sites. To do this, we compared the simulated unipolar QRS wave forms obtained with both models.

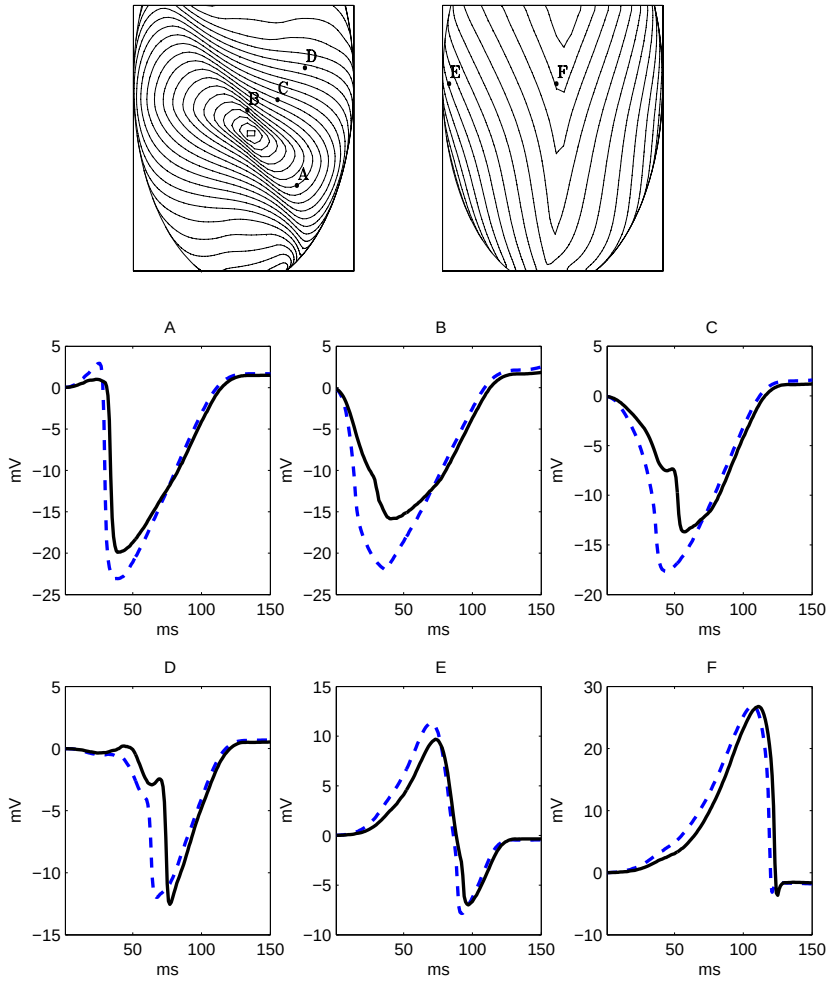

FIGURE 4. Each Panel displays epicardial unipolar electrograms (EGs) simulated in the axially isotropic case (dashed line) and in the orthotropic case (continuous line). The EGs were derived from the locations indicated by letters A - F in the upper panel.

Concerning the epicardial EGs elicited by an epicardial stimulus we have a *biphasic* waveform for sites reached by the front mainly *along fiber* while for sites *across fiber* the EGs display a *mono to tetraphasic shape* with *humps* followed by *spikes*. In fact near the stimulus site in the along fiber EGs a positive R wave appears followed by a negative going downstroke, yielding a biphasic wave shape, while the cross-fiber EGs are monophasic, i.e. present a single minimum and the portion preceeding the minimum is monotonically negative going. The negative going phase in the cross-fiber EGs is slower in the orthotropic simulation.

When about half ventricle is excited, the EG from sites close to the 80 *msec* isochrone displays a biphasic wave shape with a down-jump ranging from positive to negative values of equal magnitude (site E in Fig. 4). EGs from sites near the extinction region are entirely positive with a small negative spike after the down-jump (Panel F of Fig. 4).

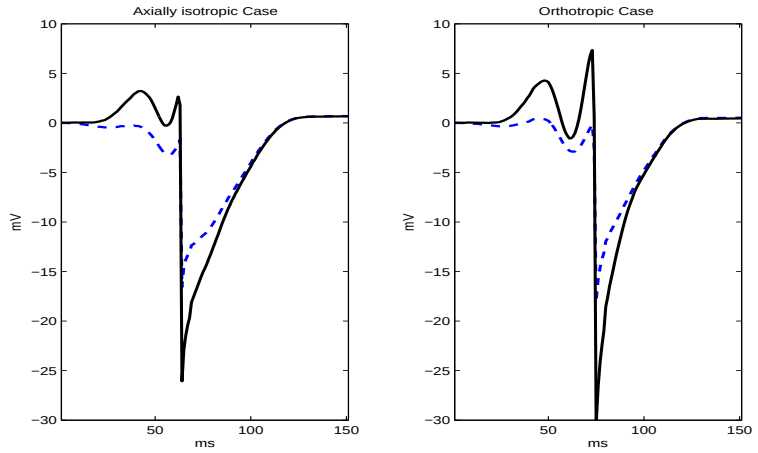

FIGURE 5. Left and rigth Panels display computed epicardial EGs related to the location of the letter C displayed in the upper Panel of Fig. 4. Left (right) Panel reports the EGs simulated in the axially isotropic (orthotropic) case computed for a ventricular wall with the endocardium in contact with blood but the epicardium is insulated (continuous line) and the EGs for site on the active epicardial tissue when the epicardium is in contact with a fluid layer (dashed line).

In conclusion the qualitative comparison of isochrones, potential maps and EGs shows that the two hypotheses *axial and orthotropic anisotropy* are both compatible with the available experimental measurements obtained during heart beats elicited by epicardial ventricular pacing. Therefore, at present, electrophysiological simulated signals that support or disprove the introduction of the proposed laminar structure of the ventricular wall [8] as a further anatomical factor that affects cross-fiber conduction, are not yet available.

References

[1] Bellettini G., Colli Franzone P. and M. Paolini. Convergence of front propagation for anisotropic bistable reaction-diffusion equations *Asymp. Anal.*, 15, 325-358, 1997.

[2] Colli Franzone, P., L. Guerri, and S. Tentoni. Mathematical modeling of the excitation process in the myocardial tissue: influence of the fiber rotation on the wavefront propagation and the potential field. *Math. Biosci.* 101: 155-235, 1990.

[3] Colli Franzone, P., L. Guerri, M. Pennacchio, and B. Taccardi. Spread of excitation in 3-D models of the anisotropic cardiac tissue.**I**:Validation of the eikonal approach. *Math. Biosci.* 113:145-209 ,1993 **II**: Effects of fiber architecture and ventricular geometry. **III**: Effects of ventricular geometry and fiber structure on the potential distribution. *Math. Biosci.* 147: 131–171, 151: 51–98, 1998.

[4] Colli Franzone, P., L. Guerri, and B. Taccardi. Potential distributions generated by point stimulation in myocariadal volume. Simulation studies in a model of anisotropic ventricular muscle. *J. Cardiovasc. Electrophysiol.* 4: 438-458, 1993.

[5] Colli Franzone P., M. Pennacchio and L. Guerri. Accurate computation of electrograms in the left ventricular wall. *Math. Mod. and Meth. in Appl. Sci.* M^3AS 10 (4): 507–538, 2000.

[6] Colli Franzone P., L. Guerri, M. Pennacchio and B. Taccardi. Anisotropic mechanisms for multiphasic unipolar electrograms. Simulation studies and experimental recordings. *Ann. Biomed. Eng.* 28: 1-17, 2000.

[7] Geselowitz D. B. On the theory of the electrocardiogram. *Proc. IEEE* 77: 857–876, 1989.

[8] LeGrice I. J., B. H. Smaill, L.Z. Chai, S.G. Edgar, J. B. Gavin and P.J. Hunter. Laminar structure of the heart: ventricular myocyte arrangement and connective tissue architecture in the dog. *Am. J. Physiol. 269 (Heart Circ. Physiol)*, 38 : H571-H582, 1995.

[9] Keener J. P. An eikonal-curvature equation for the action potential propagation in myocardium, *J. Math Biol.* 29: 629–651, 1991.

[10] Taccardi B., E. Macchi, R. L. Lux, P. R. Ershler, S. Spaggiari, S. Baruffi and Y. Vyhmeister. Effect of myocardial fiber direction on epicardial potentials, *Circulation*, 1994, 90: 3076–3090.

[11] Henriquez C. S. Simulating the electrical behavior of cardiac tissue using the bidomain model. *Crit. Rev. Biomed. Engr.* 21: 1–77, 1993.

[12] Henriquez C. S., A. L. Muzikant and C. K. Smoak. Anisotropy, fiber curvature, and bath loading effects on activation in thin and thick cardiac tissue preparations: Simulations in a three–dimensional bidomain model. *J. Cardiovasc. Electrophysiol.* 7 (5): 424–444, 1996.

[13] Simms H. D. and D. B. Geselowitz. Computation of heart surface potentials using the surface source model, *J. Cardiovasc. Electrophysiol.*, 1995, 6:522–531.

[14] Taccardi B., R. L. Lux, R. S. MacLeod, P. R. Ershler, T. J. Dustman, M. Scott, Y. Vyhmeister and N. Ingebrigtsen. Electrocardiographic waveforms and cardiac electric sources, J. Electrocardiol., 1996 29 (Suppl.): 98–100.

[15] Taccardi B., R. L. Lux,P. P. R. Ershler, R. S. MacLeod, T. J. Dustman and N. Ingebrigtsen. Anatomical architecture and electrical activity of the heart. *Acta Cardiol.*, 1997, 52 (2), 91-105.

[16] Streeter D.D. Gross morphology and fiber geometry of the heart, in : R.M. Berne (Ed.), Handbook of Physiology, Vol. 1:**The Heart, Sec. 2 : The Cardiovascular System**, Ch. 4, 61-112, Williams and Wilkins, Baltimore, MD,1979.

[17] Tomlinson K.A. Finite elements solution of eikonal equation for excitation wavefront propagation in ventricular myocardium. *Ph.D. Thesis* , The University of Auckland, New Zealand, 2000.